RIMS Kôkyûroku Bessatsu **B3**
(2007), 101–119

Ripples on icicles and stalactites

Here is a Dedication

By

Kazuto Ueno*

Abstract

Icicles and stalactites grow when their surfaces are covered with a thin film of flowing water through which latent heat of fusion and carbon dioxide are released to the surrounding air, respectively. Despite the complete difference of the basic growth mechanism, their surfaces often have ripples of centimeter-scale wavelengths. We develop a theoretical study on the morphological instability of solidification front during crystal growth from thin film of flowing water with one side being a free surface, in which we take into accout the influence of the shape of the liquid-air surface of the liquid film on the growth condition of disturbances on the solid-liquid interface.

§ 1. Introduction

When icicles are covered with a thin film of flowing water, ring-like ripples appear on the surface of icicles as seen in Figure 1 (a) [1] . In this case the temperature of ambient air is below 0° C. The mean wavelength of the ripples on natural icicles is about 8.5 mm, which do not seem to change strongly with variations in ambient air temperature, water supply rate and diameter of icicles. Figure 1 (b) is a vertical cross section of an icicle with ripples. It is observed that many tiny air bubbles are trapped in just upstream region of any protruded part of the icicle and line up in the upward direction during icicle growth [1]. This observation shows that an initial flat solid-liquid (ice-water) interface not only becomes unstable to form ripples but also moves upwards.

On the other hand, Figures 1 (c) and (d) show ice without ripples [2]. The left one in Figure 1 (c) is an icicle during sublimation and has the shape like a cone. In this case the surface of the icicle is not covered with a water layer. The right one in Figure 1 (c)

2000 Mathematics Subject Classification(s): Fluid mechanics:
Key Words: *Crystal growth, Morphological instability, Thin shear flow, Free surface*:
*Graduate School of Engineering, Nagoya University 464-8603, Japan.

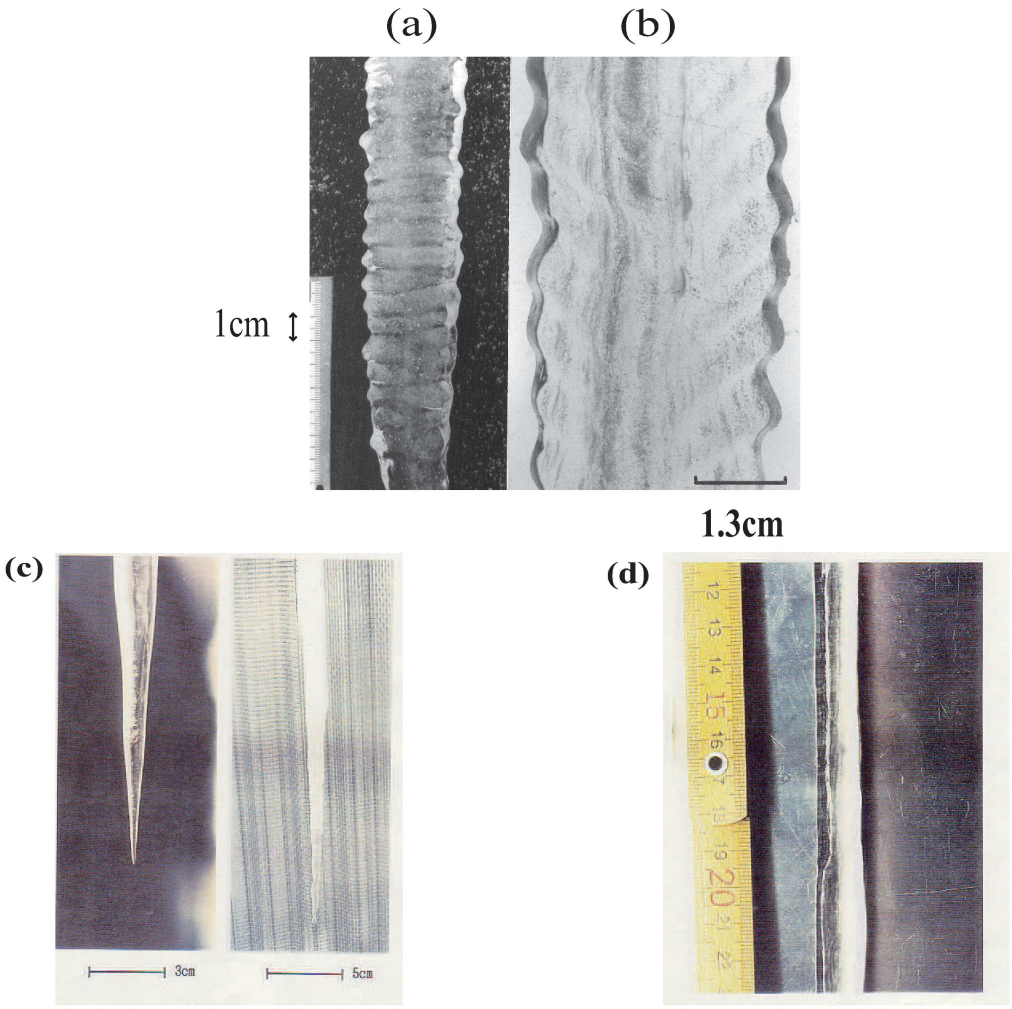

Figure 1. (a) Ripples on an icicle. (b) Vertical cross section of an icicle with ripples. (c) Icicle during sublimation (left) and melting (right). (d) Ice growth on an aluminum plate.

is an icicle during melting. The surface of the icicle is covered with a water layer due to the melting of ice by the rise of surrounding air temperature above 0° C. Figure 1 (d) shows ice growth on an aluminum plate. Since the thermal conductivity of aluminum is 236 J/(mKs), which is about 100 times greater than that of ice, most of the latent heat released at the solid-liquid interface is conducted into the aluminum through the ice. From these observations, in order to form ripples on icicles it is necessary that icicles must be covered with the supercooled water and most of the latent heat must be released through the water film into the ambient air below 0° C.

A similar ripple pattern of ice can be experimentally produced on an inclined plane set in a cold room below 0° C by continuously supplying water of nearly 0° C from the

top of the plane as sketched in Figure 2 (a) [2]. Figure 2 (b) is a vertical cross section (x, y) of the inclined plane of Figure 2 (a). The x axis is parallel to the inclined plane and the y axis is normal to it. The velocity profile in the liquid film in the unperturbed state is given by $\bar{U}(y) = u_0[2y/h_0 - (y/h_0)^2]$ [3], where h_0 is the mean thickness of the liquid film and u_0 is the surface fluid velocity. Let Q (ml/hr) and l (cm) be the volumetric water flow rate and the span width of the gutter, respectively, then the water supply rate per width is calculated from $Q/l = \int_0^{h_0} dy\bar{U}(y) = 2u_0h_0/3$. Using $u_0 = gh_0^2 \sin\theta/(2\nu)$ [3], h_0 and u_0 can be expressed as $h_0 = [2\nu/(g\sin\theta)]^{1/3}[3Q/(2l)]^{1/3}$ and $u_0 = [g\sin\theta/(2\nu)]^{1/3}[3Q/(2l)]^{2/3}$, where g is the gravitational acceleration and ν is the kinematic viscosity of the liquid. The values of h_0 and u_0 can be changed by varying Q/l or θ. In the experiment by Matsuda [2], ripples of ice were produced with different values of the angle at a fixed value of Q/l, and the average wavelength was measured for each angle. The relationship between the mean wavelength and the angle was found to be $\lambda_{\text{mean}} \sim 0.86/(\sin\theta)^{0.76}$ (cm) for Q/l =160(ml/hr)/3cm. This experimental result shows that λ_{mean} increases with decrease of the angle for a given Q/l. Since h_0 also increases with decrease of the angle, it is found that h_0 is one of the characteristic lengths in determining the wavelength of ripples.

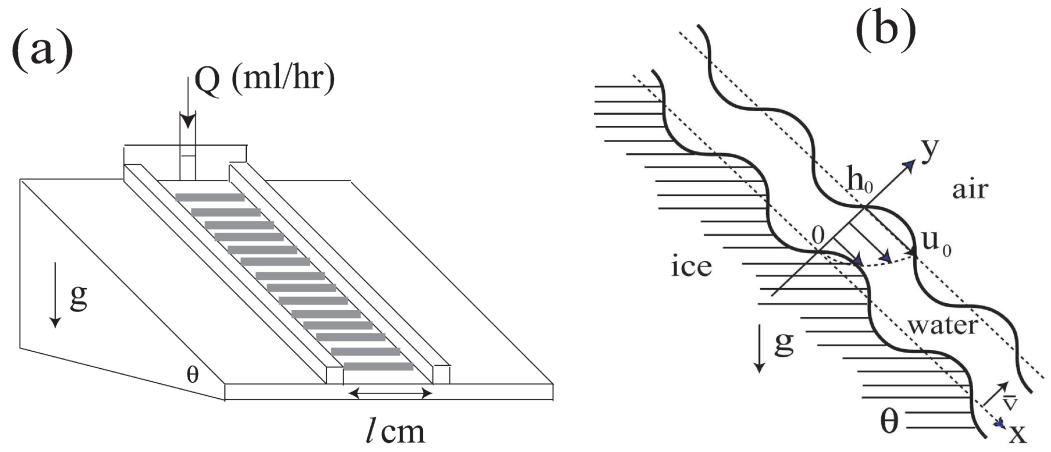

Figure 2. (a) Schematic view of experimental apparatus. Shaded stripes with nearly uniform spacing are protruded part of ripples of ice. (b) Schematic diagram of vertical cross section of the inclined plane. h_0 is the mean thickness of the liquid film and u_0 is the surface fluid velocity.

The fundamental building block of the morphological instability is the Mullins-Sekerka (MS) instability of a solidification front, which gives conditions for the growth of infinitesimal disturbances of a solid-liquid interface [4]. The dispersion relation in the MS theory for a pure material contains two characteristic lengths, which are the ther-

mal diffusion length and the capillary length associated with the solid-liquid interface tension. As a result of competition between destabilization due to thermal diffusion and stabilization due to the Gibbs-Thomson (GT) effect (the melting temperature depression due to the curvature of the interface), a pattern with a specific wavelength is developed. However, since the thickness of flowing water film on the surface of icicles is about 100 μm, the thermal diffusion layer is not formed in the liquid. Furthermore, we can neglect the GT effect because the wavelength of the ripples on icicles is about 1 cm.

To the best of our knowledge, little is known about the study on a morphological instability of solidification front during crystal growth from thin film of flowing liquid with one side being a free surface. In the growth of icicles, the transport of latent heat plays a critical role. Ice freezes when the latent heat is released through a thin film of flowing supercooled water into the ambient air below 0° C as shown in Figure 2 (b). We need to consider heat flux in each phase under appropriate boundary conditions at the solid-liquid interface and liquid-air surface. Such a theoretical attempt was firstly developed by Ogawa and Furukawa [5, 6]. They determined the wavelength of ripples quantitatively and also predicted that the ripples moves in the downward direction. However, their theoretically predicted dependence of the wavelength of the ripples on the inclined angle was not agreement with the experimental results. Furthermore, the direction of motion of ripples is opposite to the observation. We have recently proposed quite a new mechanism of the ripple formation [7, 8], in which we take into account the influence of the shape of the liquid-air surface of the liquid film on the growth condition of disturbances on the solid-liquid interface because the thickness of the liquid film is very thin. Our theoretical results are compared with those obtained by Ogawa and Furukawa, experiments and observations. We review a series of our previous papers [7, 8, 9, 10, 11] and add some recent experimental results to support our theoretical predictions. Finally, we will mention about ripples on stalactites and the surface of concrete and summarize future works to be checked by experimental observations.

§ 2. Governing equations

In the frame of reference moving at the solid-liquid interface with a mean growth rate $\bar{V}$, the equations for the temperature in the liquid T_l, solid T_s and air T_a are given by

$$\frac{\partial T_l}{\partial t} + u\frac{\partial T_l}{\partial x} + v\frac{\partial T_l}{\partial y} = \kappa_l \left(\frac{\partial^2 T_l}{\partial x^2} + \frac{\partial^2 T_l}{\partial y^2} \right), \tag{2.1}$$

$$\frac{\partial T_s}{\partial t} - \bar{V}\frac{\partial T_s}{\partial y} = \kappa_s \left(\frac{\partial^2 T_s}{\partial x^2} + \frac{\partial^2 T_s}{\partial y^2} \right), \tag{2.2}$$

$$\frac{\partial T_a}{\partial t} - \bar{V}\frac{\partial T_a}{\partial y} = \kappa_a \left(\frac{\partial^2 T_a}{\partial x^2} + \frac{\partial^2 T_a}{\partial y^2} \right), \tag{2.3}$$

where t is time, κ_l, κ_s and κ_a are the thermal diffusivities of the liquid, solid and air, respectively. Here we assume no wind in the air. u and v are the velocity components in the x and y directions and obey the Navier-Stokes equations,

$$\frac{\partial u}{\partial t} + u\frac{\partial u}{\partial x} + v\frac{\partial u}{\partial y} = -\frac{1}{\rho_l}\frac{\partial p}{\partial x} + \nu \left(\frac{\partial^2 u}{\partial x^2} + \frac{\partial^2 u}{\partial y^2} \right) + g\sin\theta, \tag{2.4}$$

$$\frac{\partial v}{\partial t} + u\frac{\partial v}{\partial x} + v\frac{\partial v}{\partial y} = -\frac{1}{\rho_l}\frac{\partial p}{\partial y} + \nu \left(\frac{\partial^2 v}{\partial x^2} + \frac{\partial^2 v}{\partial y^2} \right) - g\cos\theta, \tag{2.5}$$

and the equation of continuity,

$$\frac{\partial u}{\partial x} + \frac{\partial v}{\partial y} = 0, \tag{2.6}$$

where p is the pressure and ρ_l is the liquid density. Using the stream function ψ, u and v can be derived from $u = u_0 \partial\psi/\partial y$ and $v = -u_0 \partial\psi/\partial x$.

§ 3. Boundary conditions

Both velocity components at a disturbed solid-liquid interface $y = \zeta(t, x)$ must satisfy $u|_{y=\zeta} = 0$ and $v|_{y=\zeta} = 0$. The kinematic condition at a disturbed liquid-air surface $y = \xi(t, x)$ is $\partial\xi/\partial t + u|_{y=\xi}\partial\xi/\partial x = v|_{y=\xi}$. At the liquid-air surface the shear stress must vanish: $\partial u/\partial y|_{y=\xi} + \partial v/\partial x|_{y=\xi} = 0$ and the normal stress including the stress induced by the surface tension γ of the liquid-air surface must balance the pressure P_0 of the atmosphere: $-p|_{y=\xi} + 2\rho_l \nu \partial v/\partial y|_{y=\xi} - \gamma\partial^2\xi/\partial x^2 = -P_0$. We refer to these as the hydrodynamic boundary conditions.

The continuity of the temperature at the disturbed solid-liquid interface is $T_l|_{y=\zeta} = T_s|_{y=\zeta}$. The heat conservation at the disturbed solid-liquid interface is $L(\bar{V} + \partial\zeta/\partial t) = K_s \partial T_s/\partial y|_{y=\zeta} - K_l \partial T_l/\partial y|_{y=\zeta}$, where L is the latent heat per unit volume, and K_l and K_s are the thermal conductivities of the liquid and solid, respectively. On the other hand, the continuity of the temperature at the disturbed liquid-air surface is $T_l|_{y=\xi} = T_a|_{y=\xi} = T_{la}$, where T_{la} is a temperature at the liquid-air surface. The heat conservation at the liquid-air surface is $-K_l \partial T_l/\partial y|_{y=\xi} = -K_a \partial T_a/\partial y|_{y=\xi}$, where K_a is the thermal conductivity of the air. We refer to these as the thermodynamic boundary conditions.

§ 4. Linear stability analysis

In the following analysis, we use the values of the kinematic viscosity, $\nu = 1.8 \times 10^{-6}$ m^2/s; the density, $\rho_l = 1.0 \times 10^3$ kg/m^3; the thermal diffusivity, $\kappa_l = 1.3 \times$

$10^{-7}\mathrm{m}^2/\mathrm{s}$ of water and the surface tension of the water-air surface, $\gamma = 7.6 \times 10^{-2}$ N/m. As dimensionless numbers, we define the Reynolds number, $Re \equiv u_0 h_0/\nu = [3/(2\nu)](Q/l)$; the Peclet number, $Pe \equiv u_0 h_0/\kappa_l = [3/(2\kappa_l)](Q/l)$; the Froude number, $F \equiv u_0/(gh_0)^{1/2}$ and the Weber number, $W \equiv \gamma/(\rho_l h_0 u_0^2)$. We note that Re and Pe depend on only Q/l, while F and W depend on both Q/l and θ. For the same values of Q/l =160(ml/hr)/3cm as used in the experiment by Matsuda [2] and $\theta = \pi/2$, these dimensionless numbers take values of $Re \sim 1.23$, $Pe \sim 17.1$, $F \sim 0.79$ and $W \sim 1.42 \times 10^3$.

§ 4.1. Perturbation

We separate ξ, T_l, T_s, T_a, ψ and p into unperturbed steady fields and perturbed fields with prime as follows:

$$\begin{pmatrix} \xi(t,x) \\ T_l(t,x,y) \\ T_s(t,x,y) \\ T_a(t,x,y) \\ \psi(t,x,y) \\ p(t,x,y) \end{pmatrix} = \begin{pmatrix} h_0 \\ \bar{T}_l(y) \\ \bar{T}_s(y) \\ \bar{T}_a(y) \\ \bar{\psi}(y) \\ \bar{P}(y) \end{pmatrix} + \begin{pmatrix} \xi'(t,x) \\ T_l'(t,x,y) \\ T_s'(t,x,y) \\ T_a'(t,x,y) \\ \psi'(t,x,y) \\ p'(t,x,y) \end{pmatrix}. \tag{4.1}$$

As seen in Figure 1 (a), ring-like structure encircles the icicles and there is no noticeable variation in the azimuthal direction on their surfaces. Therefore, it is sufficient to consider only a one dimensional perturbation of the solid-liquid interface in the x direction, i.e., $\zeta(t,x) = \zeta_k \exp[\sigma t + ikx]$, where k is the wavenumber, and $\sigma = \sigma_r + i\sigma_i$, σ_r being the amplification rate and $v_p \equiv -\sigma_i/k$ being the phase velocity of the perturbation, and ζ_k is a small amplitude of the interface. We suppose that the corresponding perturbations of the liquid-air surface, the temperature of the liquid, solid, air, the stream function and pressure are expressed in the following forms:

$$\begin{pmatrix} \xi'(t,x) \\ T_l'(t,x,y) \\ T_s'(t,x,y) \\ T_a'(t,x,y) \\ \psi'(t,x,y) \\ p'(t,x,y) \end{pmatrix} = \begin{pmatrix} \xi_k \\ g_l(y) \\ g_s(y) \\ g_a(y) \\ F(y) \\ \Pi(y) \end{pmatrix} \exp[\sigma t + ikx], \tag{4.2}$$

where ξ_k, g_l, g_s, g_a, F and Π are the amplitudes of respective perturbations and they are assumed to be of the order of ζ_k.

The following calculations are based on a linear stability analysis taking into account only the first order of ζ_k. Furthermore, we use two approximations. One is

the long wavelength approximation [12]. Then we define a dimensionless wavenumber $\mu = kh_0$. For Q/l =160(ml/hr)/3cm, the value of h_0 at $\theta = \pi/2$ is about 93 μm. The value of μ is very small for the mean wavelength of the ripples on icicles. Therefore, we can neglect higher order in μ. The other is the quasi-stationary approximation. We can neglect the time dependence of perturbed temperature in each phase and that of liquid flow because these fields respond relatively rapidly to the slow development of the perturbation of solid-liquid interface.

§ 4.2. Solution of the amplitude of perturbed part of the stream function in the liquid

We substitute the assumed form of ψ' and p' into the perturbed parts of the Navier-Stokes equations (2.4) and (2.5). Under the long wavelength and quasi-stationary approximations, we obtain the Orr-Sommerfeld equation for the amplitude of perturbed part of the stream function [7]:

$$\frac{d^4 f}{dy_*^4} = i\mu Re \left\{ (2y_* - y_*^2)\frac{d^2 f}{dy_*^2} + 2f \right\}, \tag{4.3}$$

where $y_* = y/h_0$ and $F(y_*) = f(y_*)\zeta_k$. The linearized forms of the hydrodynamic boundary conditions at the solid-liquid interface and liquid-air surface can be expressed as follows:

$$\frac{df}{dy^*}\Big|_{y_*=0} = -2, \tag{4.4}$$

$$f|_{y_*=0} = 0, \tag{4.5}$$

$$f|_{y_*=1}\zeta_k = -\xi_k, \tag{4.6}$$

$$\frac{d^2 f}{dy_*^2}\Big|_{y_*=1}\zeta_k = 2\xi_k, \tag{4.7}$$

$$\frac{d^3 f}{dy_*^3}\Big|_{y_*=1}\zeta_k - i\alpha\xi_k = i\mu Re \frac{df}{dy_*}\Big|_{y_*=1}\zeta_k. \tag{4.8}$$

With these boundary conditions, we obtain an approximate solution of the Orr-Sommerfeld equation,

$$\begin{aligned} f(y_*) = & -2y_* + \frac{3(2-i\alpha)}{6-i\alpha}y_*^2 + \frac{i\alpha}{6-i\alpha}y_*^3 \\ & + \mu Re \left\{ \frac{-96\alpha - 8i\alpha^2}{105(6-i\alpha)^2}y_*^2 + \frac{4i\alpha^2}{35(6-i\alpha)^2}y_*^3 + \frac{\alpha}{15(6-i\alpha)}y_*^5 - \frac{\alpha}{30(6-i\alpha)}y_*^6 + \frac{\alpha}{210(6-i\alpha)}y_*^7 \right\}. \end{aligned} \tag{4.9}$$

In the long wavelength regions, the term with μRe in f can be neglected. From the kinematic condition at the liquid-air surface, the relation between the amplitude ξ_k of the liquid-air surface and the amplitude ζ_k of the solid-liquid interface is obtained as follows:

$$\xi_k = -f|_{y_*=1}\zeta_k \approx \frac{6}{6 - i\alpha}\zeta_k, \tag{4.10}$$

where

$$\alpha = \frac{\mu Re \cos\theta}{F^2} + \mu^3 ReW = 2\cot\theta h_0 k + \frac{2}{\sin\theta} a^2 h_0 k^3 \tag{4.11}$$

represents the restoring forces due to gravity and surface tension [12], and $a = [\gamma/(\rho_l g)]^{1/2}$ is the capillary length [3]. Since the value of W is very large as estimated above, the μ^3 term in α cannot be neglected.

Figure 3 (a) shows the dependence of the amplitude ratio $|\xi_k|/\zeta_k$ on the wavenumber k. If the liquid is water, the value of a is about 2.8 mm, which corresponds to the value of $k = 2244\ \mathrm{m}^{-1}$. In the case of $\theta = \pi/2$, the first term in α is zero. Since the value of α is small in the lower wavenumber regions in Figure 3 (a), the effect of restoring force due to the surface tension on the liquid-air surface can be neglected and then the amplitude of the liquid-air surface is almost the same as that of the solid-liquid interface. When the wavelength of a disturbance of the solid-liquid interface is greater than a, fluid flows down along the disturbed solid-liquid interface as shown in Figure 3 (b). On the other hand, since the value of α is large in the higher wavenumber regions in Figure 3 (a), the effect of the surface tension on the liquid-air surface is effective and then the shape of the liquid-air surface tends to be flat against the disturbed solid-liquid interface as shown in Figure 3 (c). When the wavelength of a disturbance of the solid-liquid interface is smaller than a, fluid tends to flow down without feeling the disturbed solid-liquid interface. Furthermore, we can see a small phase shift of the liquid-air surface in the upward direction against the solid-liquid interface. Consequently, the capillary length a is an important characteristic length to determine the shape of the liquid-air surface. For $\theta \neq \pi/2$, beside the surface tension, the gravity also acts on the liquid-air surface as the restoring force, which is represented by the first term in α [9].

§ 4.3. Solution of the amplitude of perturbed part of the temperature in the liquid

The perturbed parts of equation (2.1) of temperature in the liquid is

$$\frac{\partial T_l'}{\partial t} + \bar{U}(y)\frac{\partial T_l'}{\partial x} + v'\frac{\partial \bar{T}_l}{\partial y} = \kappa_l \left(\frac{\partial^2 T_l'}{\partial x^2} + \frac{\partial^2 T_l'}{\partial y^2} \right). \tag{4.12}$$

We substitute the assumed forms of T_l' and ψ' into equation (4.12). Under the long wavelength and quasi-stationary approximations and introducing a new variable $z =$

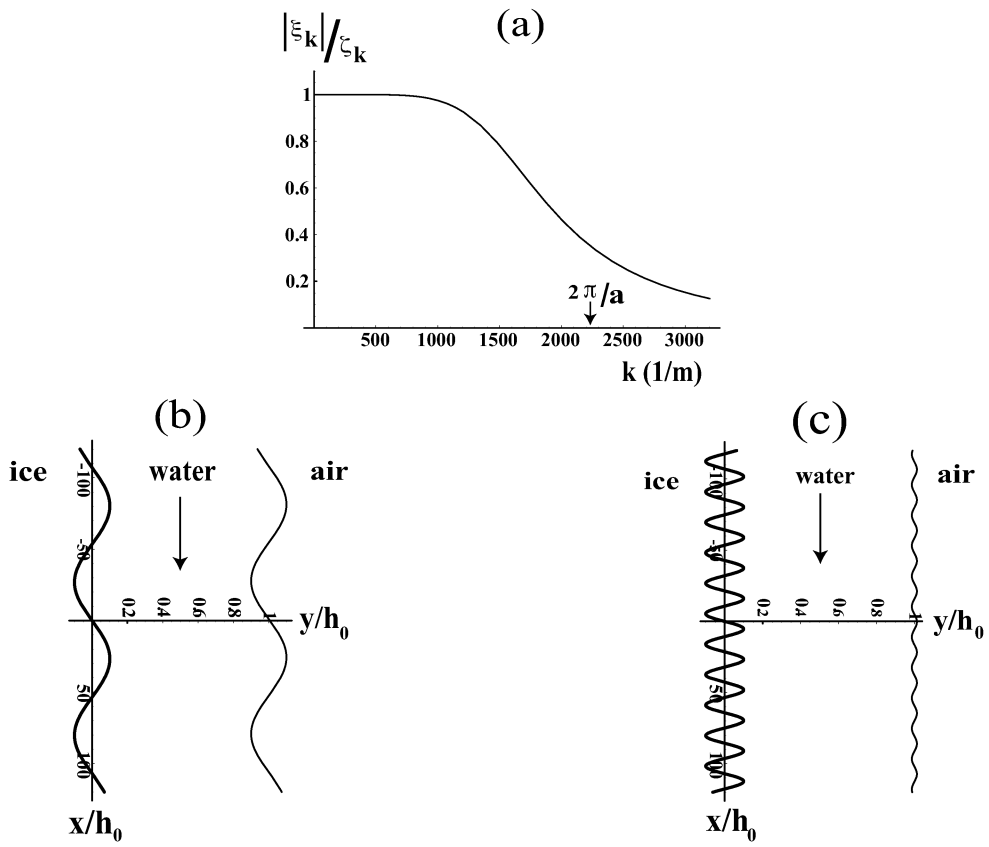

Figure 3. For Q/l =160(ml/hr)/3cm and $\theta = \pi/2$, (a) the amplitude ratio $|\xi_k|/\zeta_k$ on the wavenumber k. a is the capillary length. The shape of the water-air surface (solid line) for a disturbed ice-water interface (thick solid line) with a amplitude $\zeta_k/h_0 = 0.1$ when the wavelength of (b) 1 cm ($k \sim 628$ m^{-1}) and (c) 2 mm ($k \sim 3142$ m^{-1}).

$1 - y_*$, we obtain the equation for the amplitude of perturbed part of the temperature in the liquid [7]:

$$\frac{d^2 g_l}{dz^2} - i\mu Pe(1 - z^2)g_l = i\mu Pe f(z)\bar{G}_l \zeta_k, \tag{4.13}$$

where $\bar{G}_l \equiv -d\bar{T}_l/dy|_{y=0}$ is unperturbed part of the temperature gradient in the liquid film and $\bar{G}_l > 0$ means that water is in supercooled state. The second term of the left hand side and the right hand side of the equation (4.13) are originated from the mean shear flow $\bar{U}$ and the perturbation of normal velocity, $v' = -u_0 \partial\psi'/\partial x$, generated from a disturbance of the solid-liquid interface, respectively. We can say that in the long wavelength regions the perturbed part of heat transport in the liquid is dominated by these flows. Using the linearized forms of the thermodynamic boundary conditions at

the liquid-air surface, we obtain an approximate solution for g_l [7]:

$$g_l(z) = \left[-f|_{z=0} \left\{ \phi_1(z) + \mu\phi_2(z) \right\} + i\mu Pe \int_0^z \left\{ \phi_2(z)\phi_1(z') - \phi_1(z)\phi_2(z') \right\} f(z')dz' \right] \bar{G}_l\zeta_k \\ \equiv H_l(z)\bar{G}_l\zeta_k, \tag{4.14}$$

where $\phi_1(z)$ and $\phi_2(z)$ are two independent homogeneous solutions of equation (4.13) and are given by

$$\phi_1(z) = 1 + i\left(\frac{1}{2}z^2 - \frac{1}{12}z^4\right)\mu Pe + \left(-\frac{1}{24}z^4 + \frac{7}{360}z^6 - \frac{1}{672}z^8\right)(\mu Pe)^2 + \cdots, \tag{4.15}$$

$$\phi_2(z) = z + i\left(\frac{1}{6}z^3 - \frac{1}{20}z^5\right)\mu Pe + \left(-\frac{1}{120}z^5 + \frac{13}{2520}z^7 - \frac{1}{1440}z^9\right)(\mu Pe)^2 + \cdots, \tag{4.16}$$

which are expressed in the expansion in terms of μPe. Since $\mu Pe \sim O(1)$ for the wavelength of ripples on icicles, it is sufficient to consider up to the first term in μPe of equations (4.15) and (4.16) in the following calculations because the coefficients in front of higher order terms in μPe are very small [10].

§ 4.4. Dispersion relation

We substitute the assumed form of T_l' and T_s' into the perturbed part of the thermodynamic boundary conditions at the solid-liquid interface and linearize them at $y_* = 0$. Then we can obtain the dispersion relation for the fluctuation of the solid-liquid interface:

$$\sigma = \frac{\bar{V}}{h_0}\left\{ \left.\frac{dH_l}{dz}\right|_{z=1} + n\mu(H_l|_{z=1} - 1) \right\}. \tag{4.17}$$

The amplification rate σ_r and the phase velocity $v_p = -\sigma_i/k$ are obtained from the real and imaginary part of σ, respectively, [7]

$$\sigma_r = \frac{\bar{V}}{h_0}\left[\frac{-\frac{3}{2}\alpha(\mu Pe) + \mu\left\{36 - \frac{3}{2}\alpha(\mu Pe)\right\}}{36 + \alpha^2} + n\mu\frac{-\frac{7}{10}\alpha(\mu Pe) - \alpha^2 + \mu\left\{36 - \frac{7}{10}\alpha(\mu Pe)\right\}}{36 + \alpha^2} \right], \tag{4.18}$$

$$v_p = -\frac{\bar{V}}{\mu}\left[\frac{-\frac{1}{4}\alpha^2(\mu Pe) + \mu\left\{6\alpha + 9(\mu Pe)\right\}}{36 + \alpha^2} + n\mu\frac{6\alpha - \frac{7}{60}\alpha^2(\mu Pe) + \mu\left\{6\alpha + \frac{21}{5}(\mu Pe)\right\}}{36 + \alpha^2} \right]. \tag{4.19}$$

Figure 4 (a) shows the amplification rate σ_r versus the wavenumber k. Our result is shown by the solid line. An experimental observation shows that the increase in wind speed in the air or the decrease in ambient air temperature lead to the increase in $\bar{V}$ [1]. Although the change in $\bar{V}$ due to such environmental conditions affects the magnitude of σ_r, the wavenumber at which σ_r takes a maximum value does not change. From this wavenumber we define the wavelength of ripples as $\lambda_{\max}$. It is reported in the experiment that a periodic structure as the original form of ripples of ice is observed in about 30 minutes [2]. The characteristic time for the most unstable mode in Figure 4 (a) can be estimated from σ_r^{-1} and is about 30 minutes for typical mean growth rate of $\bar{V} = 10^{-6}$ m/s [1]. The characteristic time predicted from the theory is in good agreement with the experimental result.

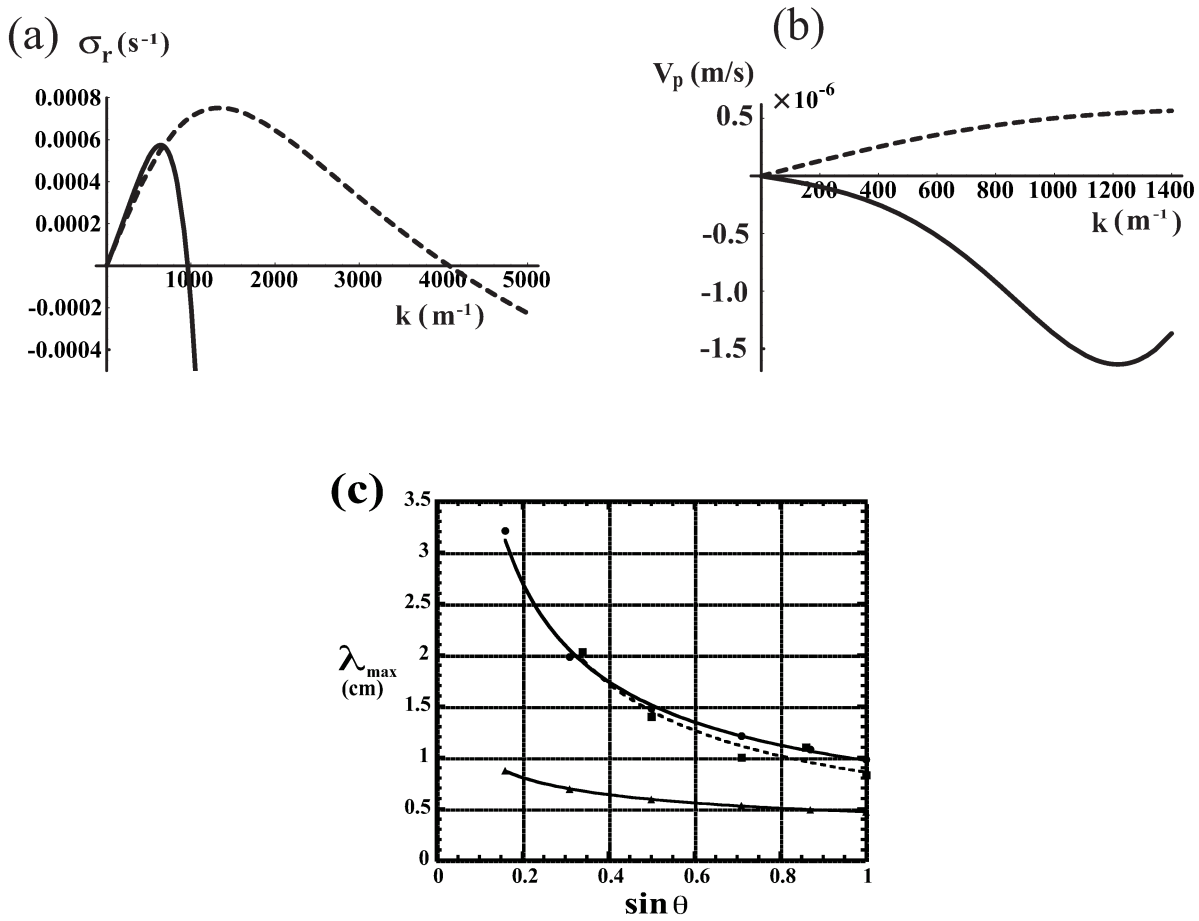

Figure 4. For $\bar{V} = 10^{-6}$ m/s and Q/l =160(ml/hr)/3cm, (a) the amplification rate σ_r vs the wavenumber k at $\theta = \pi/2$. (b) the phase velocity v_p vs the wavenumber k at $\theta = \pi/2$. (c) the dependence of wavelength $\lambda_{\max}$ on $\sin\theta$. Experiment by Matsuda, ■; Ueno's theory, ●; Ogawa and Furukawa's theory, ▲.

Figure 4 (b) shows the phase velocity v_p versus the wavenumber k. Our result is shown by the solid line. If we estimate the value of v_p at the wavenumber at which σ_r takes a maximum value in Figure 4 (a), the value is about $-0.6\ \bar{V}$. Figure 5 shows schematic view of the time evolution of the solid-liquid interface, $\mathrm{Im}[\zeta/h_0] = \sin[k(x - v_p t)]\exp(\sigma_r t)\zeta_k/h_0$, where the values of $\sigma_r = 6.0 \times 10^{-4}$ s^{-1} and $v_p = -0.6 \times 10^{-6}$ m/s determined above are used. The negative sign of v_p means that the solid-liquid interface moves in the upward direction, which is consistent with the observation of line up in the upward direction of air bubbles trapped in icicle as shown in Figure 1 (b). Recently, a preliminary experiment has been done by Morris in the cold room at DAMTP, University of Cambridge, to see if the motion of the ripples could be observed. You can see the detailed movies in his web page [13].

Figure 4 (c) shows the dependence of the wavelength $\lambda_{\max}$ on $\sin\theta$. Our theoretical result (●), $\lambda_{\max} \sim 0.97/(\sin\theta)^{0.64}$ (cm), are obtained by varying the value of $\sin\theta$ and $\cot\theta$ involved in σ_r, which is in good agreement with the experimental results (■), $\lambda_{\mathrm{mean}} \sim 0.86/(\sin\theta)^{0.76}$ (cm) by Matsuda.

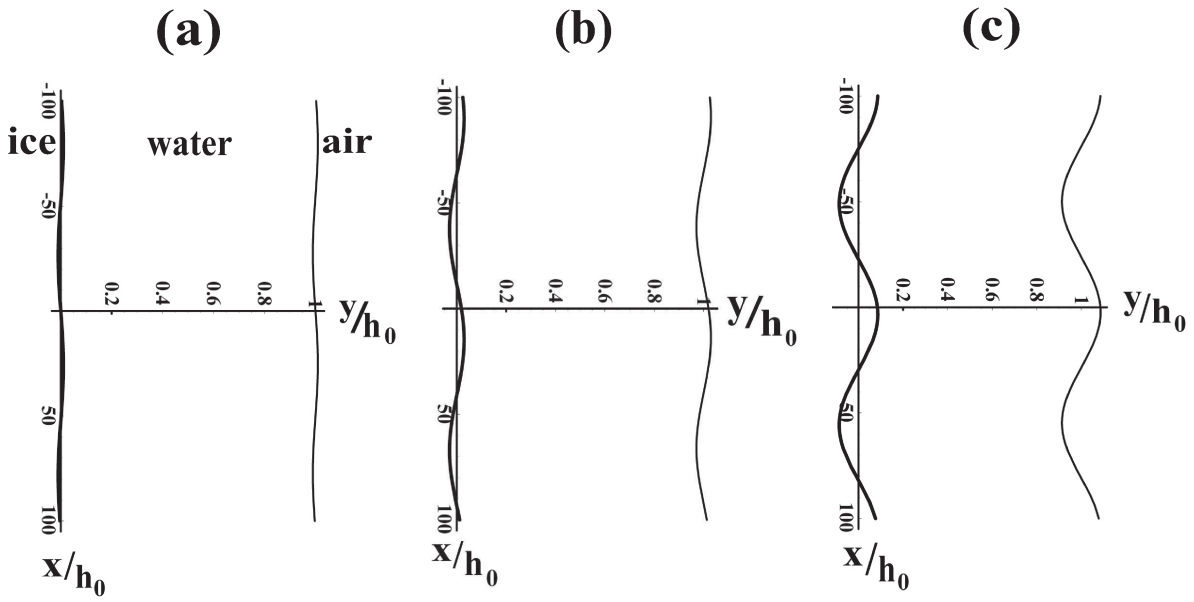

Figure 5. Schematic view of time evolution of the solid-liquid interface. (a) Initial amplitude ζ_k/h_0 at $t = 0$ is 0.01. (b) t=0.5 hr. (c) t=1.0 hr.

It should be noted that there are some differences between our theory and the Ogawa and Furukawa's theory. One is the difference in the thermodynamic boundary conditions. In the Ogawa and Furukawa's theory, $T_l|_{y=\zeta} = T_s|_{y=\zeta} = T_m$ and $T_l|_{y=\xi} = T_a|_{y=\xi}$ are imposed at the solid-liquid interface and liquid-air surface, respectively, where T_m is the equilibrium melting temperature. The other is the difference in the shape of

the liquid-air surface. In the Ogawa and Furukawa's theory, since the effect of the restoring forces due to gravity and surface tension on the liquid-air surface is neglected, i.e. $\alpha = 0$, the shape of the liquid-air surface have the same amplitude as that of the solid-liquid interface and phase difference between them does not occur. Taking into account these differences, we can easily derive their dispersion relation from our theoretical formalism [8]. The results are

$$\sigma_r = \bar{V}k\frac{1-\frac{239}{10080}(\mu Pe)^2}{\left\{1-\frac{239}{10080}(\mu Pe)^2\right\}^2+\left(\frac{5}{12}\mu Pe\right)^2}, \tag{4.20}$$

$$v_p = \bar{V}\frac{\frac{5}{12}(\mu Pe)}{\left\{1-\frac{239}{10080}(\mu Pe)^2\right\}^2+\left(\frac{5}{12}\mu Pe\right)^2}. \tag{4.21}$$

Their results are shown in the dashed lines in Figures 4 (a) and (b). They obtained $5 \sim 13$ mm for the wavelength of ripples [5]. However, this claim is lack of theoretical foundation. The experiment by Matsuda was done at only Q/l =160(ml/hr)/3cm [2]. At this value and $\theta = \pi/2$, the mean thickness of the liquid film is 93 μm, which is uniquely determined from the equation $h_0 = [2\nu/(g\sin\theta)]^{1/3}[3Q/(2l)]^{1/3}$. Then the wavelength of 5 mm is obtained from the equation (4.20). Nevertheless, they assumed the thickness to be in the range of $93 \sim 121$ μm from the first and obtained the wavelength in the range of $5 \sim 13$ mm. It is impossible to get this range of wavelength for the fixed value of Q/l. In fact, there is no experimental evidence to support the Ogawa and Furukawa's theoretical results. First, the dependence of the wavelength $\lambda_{\max}$ on $\sin\theta$ in their theory, $\lambda_{\max} \sim 0.47/(\sin\theta)^{1/3}$ (cm), is deviated from the experimental result (■) as shown by ▲ in Figure 4 (c). There is other experimental report that $\lambda_{\mathrm{mean}} \propto 1/(\sin\theta)^{0.62\pm0.11}$, which also does not support the Ogawa and Furukawa's result [14]. Since σ_r in the Ogawa and Furukawa's theory does not include α, the behavior of the dependence of $\lambda_{\max}$ on $\sin\theta$ is different from ours. Their σ_r includes only one characteristic length h_0. Since $h_0 \propto 1/(\sin\theta)^{1/3}$, that is why their $\lambda_{\max}$ is proportional to $1/(\sin\theta)^{1/3}$. Secondly, the sign of the phase velocity shown by the dashed line in Figure 4 (b) is opposite to that of our result, the observation in Figure 1 (b) and the experiment [13].

§ 5. Mechanism of destabilization and/or stabilization and movement of the solid-liquid interface

In Figures 6 (a) and (b), thick solid lines represent the solid-liquid interface $\mathrm{Im}[\zeta/h_0] = \sin[k(x-v_pt)]\exp(\sigma_r t)\zeta_k/h_0$ and the liquid-air surface $1 + \mathrm{Im}[\xi/h_0]$. Thick dashed lines are distributions of net heat flux $q_l - q_s$ at $\mathrm{Im}[\zeta/h_0]$ and that of heat flux q_a at $1 + \mathrm{Im}[\xi/h_0]$, where q_l, q_s and q_a are defined by $q_l \equiv \mathrm{Im}[-K_l\partial T_l'/\partial y|_{y=\zeta}]$, $q_s \equiv$

$\mathrm{Im}[-K_s\partial T_s'/\partial y|_{y=\zeta}]$ and $q_a \equiv \mathrm{Im}[-K_a\partial T_a'/\partial y|_{y=\xi}]$. Here Im denotes the imaginary part of its argument. From the thermodynamic boundary conditions at the solid-liquid interface, we can express $q_l - q_s = L|\sigma|\sin[k(x - v_p t) - \phi]\exp(\sigma_r t)\zeta_k$, where $|\sigma| = \sqrt{\sigma_r^2 + \sigma_i^2}$, $\sigma_r = |\sigma|\cos\phi$, $\sigma_i = -|\sigma|\sin\phi$, and ϕ is a phase difference between $q_l - q_s$ and $\mathrm{Im}[\zeta/h_0]$. Since the thick dashed lines are shifted in the upward direction against the thick solid lines, it is found that $\phi < 0$. Then $\sigma_i > 0$ and $v_p = -\sigma_i/k < 0$. The negative sign of v_p is consistent with that of the solid line in Figure 4 (b).

First, we consider the case of $-\pi/2 < \phi < 0$ in Figure 6 (a). This is the distribution at the wavenumber of $k = 628\ \mathrm{m}^{-1}$, at which $\sigma_r > 0$ as shown by the solid line in Figure 4 (a). In unperturbed state, we assume that $T_s = 0°$ C in the ice and the temperature at the water-air surface is T_{la}. Its value is about $-0.06°$ C from the heat continuity equation when $\bar{V} = 10^{-6}$ m/s. After the interface is perturbed, the temperature over the water-air surface remains at $T_{la} = -0.06°$ C, while the temperature of the ice-water interface is not necessary to be kept at $T_m = 0°$ C. In fact, we can see extremely small deviation of temperature from $T_m = 0°$ C in Figures 6 (a) and (b), and the deviation is much greater than the change in T_m due to the curvature effect of the solid-liquid interface. Consequently, there is heat flow q_s from the solid-liquid interface to the ice in the regions of $T_s > T_m$, while there is heat flow q_s from the ice to the interface in the regions of $T_s < T_m$. This deviation effect of temperature from $T_m = 0°$ C is reflected in the second terms in equations (4.18) and (4.19). The amplitude of q_a is the largest at the protruded part of $\mathrm{Im}[\xi/h_0]$. The thermal diffusion into the air is the largest at this point because the temperature gradient is the largest. Since the value of α is small at this wavenumber, the amplitudes of both interfaces are almost the same and phase difference between them cannot be seen. Therefore, it seems to grow fastly at the protruded part of the solid-liquid interface. However, since actual distribution of $q_l - q_s$ is shifted in the upward direction by ϕ against $\mathrm{Im}[\zeta/h_0]$, the temperature gradient is not the largest at the protruded part of the solid-liquid interface. The mean growth rate of solidification is given by $\bar{V} = K_l\bar{G}_l/L$. In the region of $q_l - q_s > 0$, where the total heat flux is greater than the mean heat flux $K_l\bar{G}_l$, the growth rate of the solid-liquid interface is greater than $\bar{V}$ and then the interface grows fastly. On the other hand, in the region of $q_l - q_s < 0$, where the total heat flux is smaller than $K_l\bar{G}_l$, the growth rate of the solid-liquid interface is smaller than $\bar{V}$ and then the interface grows slowly. In the configuration shown in Figure 6 (a), in just the upstream region of any protruded part of the solid-liquid interface, interface grows faster, while in just the downstream region of any protruded part of the solid-liquid interface, interface grows slowly. As a result, the solid-liquid interface not only becomes to be unstable but also moves in the upward direction. This is consistent with the sign of the phase velocity obtained from our result. It should be noted that the mechanism proposed here cannot be explained

by the Laplace instability discussed in the Ogawa and Furukawa's theory.

Second, we consider the case of $-\pi < \phi < -\pi/2$ in Figure 6 (b). This shows the distribution at the wavenumber of $k = 1256$ m^{-1}, at which $\sigma_r < 0$ as shown by the solid line in Figure 4 (a). Since the value of α is large at this wavenumber, we can see that the phase of $\mathrm{Im}[\xi/h_0]$ and q_a is slightly shifted in the upward direction against $\mathrm{Im}[\zeta/h_0]$. In this configuration, $q_l - q_s < 0$ at the protruded part of the solid-liquid interface and then the interface grows slowly, while $q_l - q_s > 0$ at the depression part of it and then the interface grows fastly. Consequently, the interface will tend to be flat and ripples of short wavelengths disappear. This is a new mechanism of stabilization of the solid-liquid interface completely different from the discussion given in the Ogawa and Furukawa's theory.

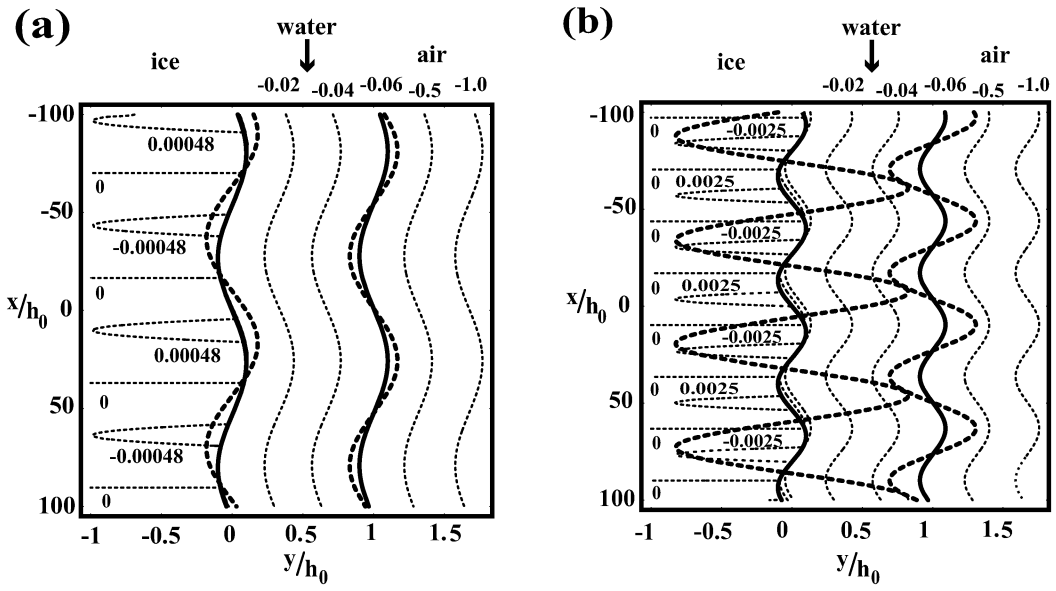

Figure 6. Thick solid lines are the solid-liquid interface $\mathrm{Im}[\zeta/h_0]$ and the liquid-air surface $1 + \mathrm{Im}[\xi/h_0]$; thick dashed lines are distribution of heat flux $q_l - q_s$ at $\mathrm{Im}[\zeta/h_0]$ and distribution of heat flux q_a at $1 + \mathrm{Im}[\xi/h_0]$. (a) The wavenumber in the unstable region ($k = 628$ m^{-1}). (b) The wavenumber in the stable region ($k = 1256$ m^{-1}). Thin dashed lines are isotherm.

§ 6. Ripples on speleothems and concrete

In the growth of icicle, the transport of the latent heat plays a critical role. On the other hand, in the growth of stalactite, the transport of CO_2 plays a critical role. $CaCO_3$ precipitates when CO_2 is released from a thin film of flowing supersaturated solution of Ca^{2+} and HCO_3^- into the lower partial pressure of CO_2 in the cave [15, 16, 17]. Figure 7

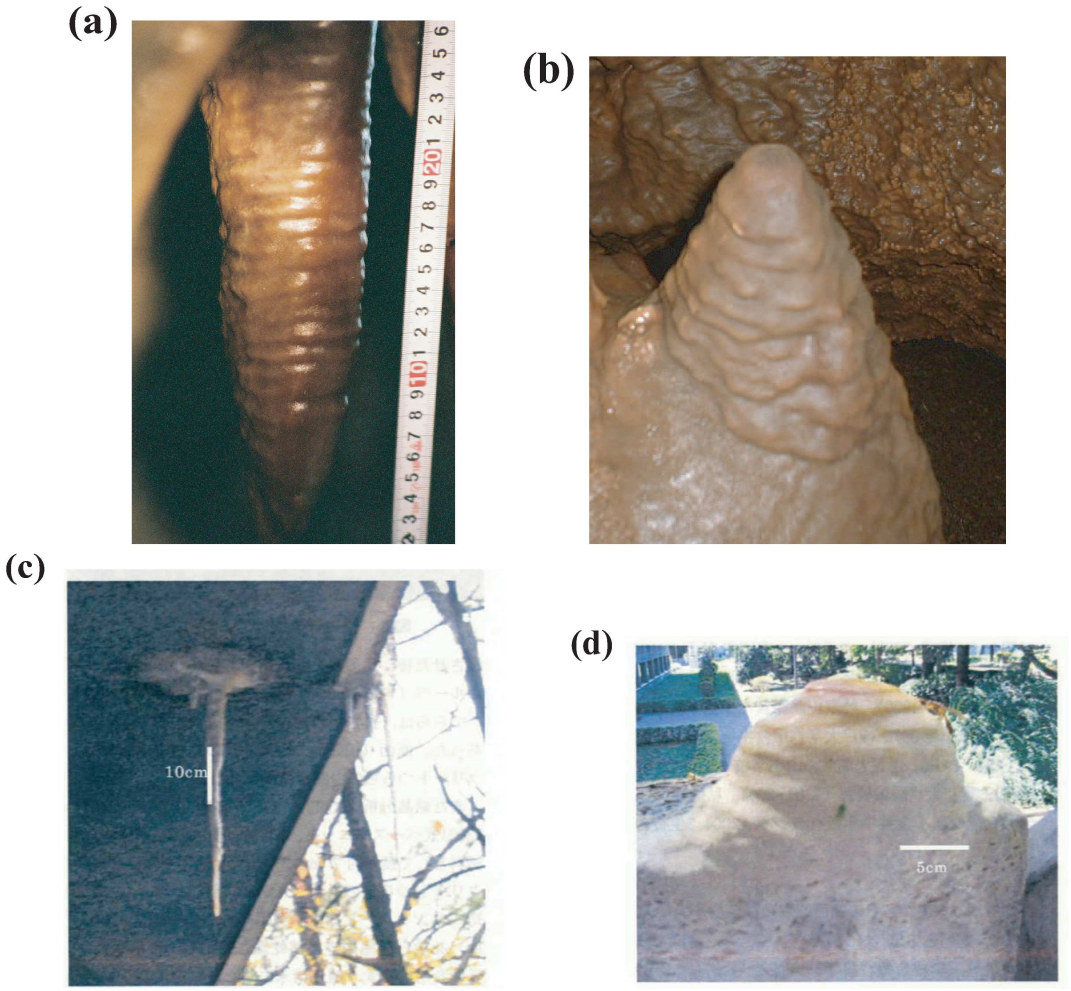

Figure 7. (a) Ripples on an stalactite. (b) Stalagmite. (c) Concrete stalactite. (d) Concrete stalagmite.

(a) shows stalacites in the Ohtaki limestone cave, Japan. Stalactite grows from a portion of the flowing water layer covering their surfaces. The rest of the water drips from their tip. As shown in Figure 7 (b), a stalagmite is often formed from the remainig water dripping from a stalacite. Figures 7 (c) and (d) show a concrete stalactite and stalagmite [18]. A liquid leaks from the ceiling of a concrete building. This liquid is supersaturated solution of Ca^{2+} and HCO_3^- by dissolution of $CaCO_3$ included in concrete at the top by water being enriched in dissolved CO_2. $CaCO_3$ precipitates from this solution by a reaction $Ca^{2+} + 2HCO_3^- \rightarrow CaCO_3 + H_2O + CO_2$ by outgassing CO_2. This mechanism is the same as formation of stalactites in the limestone cave. Surprisingly, despite the difference in the basic growth mechanism between icicles and stalactites, the surfaces on stalactites and stalagmites also have ripples of centimeter-scale wavelengths. We have recently constructed a theoretical framework for ripple formation on stalactites under the assumption that the mean concentration distribution of CO_2 in liquid film is linear [19]. We have obtained the centimeter-scale wavelength for the ripples of calcium carbonate from the most unstable mode of the interface. Its characteristic time of appearence of periodic structure, the magnitude and direction of movement velocity of ripples can be predicted like icicles. These theoretical predictions should be checked by experimental observations in the near future.

§ 7. Summary

A new theory on the morphological instability of solidification front in crystal growth from thin flowing liquid with one side being a free surface was presented. We took into account the effect of restoring forces due to gravity and surface tension on the shape of the liquid-air surface. According to our theory, the destabilization and/or stabilization of the solid-liquid interface is found to be related to the magnitude of phase difference between a disturbed solid-liquid interface and distribution of heat flux on it. The direction of the phase shift of the distribution of heat flux against the solid-liquid interface is related to the direction of movement of the solid-liquid interface. The dispersion relation derived from our theory contains two characteristic lengths. One is the thickness of the liquid film and the other is the capillary length associated with the surface tension of the liquid-air surface. These characteristic lengths are important factors to determine the wavelength of the ripples on icicles.

Some of our theoretical predictions were in good agreement with experiments for a fixed water supply rate per width, Q/l. However, our other theoretical predictions should be checked through experiments. For example, (1) Our theory predicts that the wavelength of ripples increases gradually with Q/l. However, the actual experiment by Matsuda shows that ice itself does not grow and ripples are not formed when the water supply rate is too small or too large. There may be an appropriate range of Q/l

to clearly form ripples. Our theory cannot explain this fact. It needs to measure the wavelength for various Q/l and modify the present theory into a form which takes into account the dependence of the mean growth rate $\bar{V}$ of icicles on the water supply rate. (2) The experiment done by Morris at DAMTP shows that ripples on icicles do move in the upward direction as predicted by our theory. It needs to measure precise velocity of the motion of the ripples under carefully control of Q/l and air temperature. (3) In our theory, the capillary length associated with the surface tension of the liquid-air surface is one of the important characteristic lengths in determining the wavelength of ripples. Our theory predicts that the wavelength of ripples becomes shorter with the reduction of the surface tension. It needs to measure the wavelength of ripples when reducing the surface tension of water by adding a surfactant.

Acknowledgements

The author would like to thank N. Maeno, S. Matsuda and A. Onodera for providing pictures of Figures 1 (a), (b) , Figures 1 (c), (d) and Figures 7 (c), (d), respectively. The author would also like to thank H. Shoyama for assistance in photographing speleothems in the Ohtaki limestone cave. This work was supported by a Grant-in-Aid for the 21st Century COE "Frontiers of Computational Science".

References

[1] Maeno, N., Makkonen, L., Nishimura, K., Kosugi, K. and Takahashi, T., Growth rates of icicles, *J. Glaciol.*, **40** (1994), 319-326.
[2] Matsuda, S., Experimental study on the wavy pattern of icicle's surface, Master's thesis, Institute of Low Temperature Science, Hokkaido University, 1997.
[3] Landau, L. and Lifschitz, E., *Fluid Mechanics*, Pergamon Press, NewYork, 1959.
[4] Mullins, W. W. and Sekerka, R. F., Morphological stability of a particle growing by diffusion or heat flow, *J. Appl. Phys.*, **34** (1963), 323-329.
[5] Ogawa, N. and Furukawa, F., Surface instability of icicles, *Phys. Rev. E*, **66** (2002), 041202.
[6] Schewe, P., Riordon, J. and Stein, B., Icicle Instability, *Physics News Update Number*, 613, November 13, 2002.
[7] Ueno, K., Pattern formation in crystal growth under parabolic shear flow, *Phys. Rev. E*, **68** (2003), 021603.
[8] Ueno, K., Pattern formation in crystal growth under parabolic shear flow II, *Phys. Rev. E*, **69** (2004), 051604.
[9] Ueno, K., Characteristics of the wavelength of ripples on icicles, submitted.
[10] Ueno, K., Ripples on the Surface of Icicles (in Japanese), *J. Jpn. Soc. Fluid Mech. (Nagare)*, **25** (4) (2006), 381-389.
[11] Ueno, K. and Maeno, N., Ripple formation mechanism on icicles under a thin shear flow, in *Physics and Chemistry of Ice*, edited by Kuhs, W. F., Royal Society of Chemistry, Cambridge, (2007), 619-626

[12] Benjamin, T. B., Wave formation in laminar flow down an inclined plane, *J. Fluid Mech.*, **2**, (1957), 554-574.
[13] http://www.physics.utoronto.ca/~smorris/edl/icicleripples/icicleripples.html
[14] http://physics.valpo.edu/colloquia/colloq_041604.html
[15] Buhmann, D. and Dreybrodt, W., The kinetics of calcite dissolution and precipitation in geologically relevant situations of karst areas 1. open system, *Chem. Geol.*, **48**, (1984), 189-211.
[16] Short, M. B., Baygents, J. C., Beck, J. W., Stone, D. A., Toomey III, R. S. and Goldstein, R. E., Stalactite growth as a free-boundary problem: a geometric law and its platonic ideal, *Phys. Rev. Lett.*, **94**, (2005), 018501.
[17] Short, M. B., Baygents, J. C., and Goldstein, R. E., Stalactite growth as a free-boundary problem, *Phys of Fluids*, **17**, (2005), 083101.
[18] Onodera, A. and Okazaki, M., A basic study on development of teaching material using concrete icicles -models of biocalcification mechanism and atmospheric CO_2 cycling through lime stone, *Bull. Tokyo Gakugei Univ. Natur. Sci.*, **57**, (2005). 41-56.
[19] Ueno, K., What determines the wavelength of ripple on icicles and stalactites?, to be submitted